Possible overestimation of shallow-depth calcium carbonate dissolution in the ocean

K. Friis,[1,2] R. G. Najjar,[1] M. J. Follows,[3] and S. Dutkiewicz[3]

Received 26 March 2006; revised 13 August 2006; accepted 18 September 2006; published 28 December 2006.

[1] We argue that diagnostics of excess dissolved calcium carbonate (TA*) above the saturation horizon cannot be unambiguously interpreted in terms of local in situ dissolution. We examine a three-dimensional numerical model of global ocean circulation and biogeochemistry with explicit representation of the formation and dissolution of calcium carbonate. In particular, dissolution is only allowed to occur below the saturation horizon. The model qualitatively captures the observed basin- and global-scale patterns of alkalinity and TA* as well as the relationship between TA* and chlorofluorocarbon age in the thermocline. The existence of TA* above the saturation horizon in the model can only be explained in terms of transport subsequent to dissolution. The model study does not rule out the possibility of shallow-depth calcium carbonate dissolution but suggests that dissolution rates derived from tracer observations have not adequately accounted for the influence of transport.

Citation: Friis, K., R. G. Najjar, M. J. Follows, and S. Dutkiewicz (2006), Possible overestimation of shallow-depth calcium carbonate dissolution in the ocean, *Global Biogeochem. Cycles*, *20*, GB4019, doi:10.1029/2006GB002727.

1. Introduction

[2] Calcifying plankton, such as coccolithophorids, produce calcium carbonate in the euphotic zone. This particulate inorganic carbon is subsequently exported to depth as gravitationally sinking detritus. A long-standing paradigm is that calcium carbonate particles sink unaffected through the upper ocean, which is supersaturated with respect to $CaCO_3$, and only dissolve below the saturation horizon, where the waters are undersaturated with respect to $CaCO_3$ [e.g., *Broecker and Peng*, 1982, pp. 84–89]. In most regions of the ocean this only occurs below 1000 m. Recently, however, there have been suggestions that shallow-depth calcium carbonate dissolution (i.e., in situ dissolution above the saturation horizon) may occur in the open ocean [*Anderson and Sarmiento*, 1994; *Lohmann*, 1995; *Milliman and Droxler*, 1996; *Milliman et al.*, 1999; *Schiebel*, 2002]. Such dissolution would be significant for our understanding of the global ocean carbon cycle. It implies a shorter timescale for the cycling of calcium carbonate within the ocean and thus has significant implications for feedbacks between climate, atmospheric CO_2, and the marine carbon cycle.

[3] A discussion of $CaCO_3$ dissolution is aided by an examination of alkalinity, which is readily measured and substantially influenced by dissolution. The total alkalinity, TA, of a water parcel may be discussed in terms of three components,

$$TA = TA^{o} + 2\ TA^{*} + TA^{AOU}, \quad (1)$$

where TA^{o} is the preformed alkalinity, which is the value of alkalinity as the water parcel leaves the surface ocean; TA* (called ΔTA^{CaCO3} by *Chung et al.* [2003] and $\Delta CaCO_3$ by *Feely et al.* [2004]), is the sub-surface increase in the dissolved calcium concentration due to the dissolution of $CaCO_3$ (the factor of two converts one mole of $CaCO_3$ to two equivalents of alkalinity); and TA^{AOU} is a minor contribution due to the remineralization of organic matter at depth [*Brewer*, 1978; *Feely et al.*, 2002].

[4] Several recent studies have diagnosed TA* from large-scale ocean observations and interpreted its presence above the saturation horizon as a signature of shallow-depth dissolution of $CaCO_3$ [*Feely et al.*, 2002; *Sabine et al.*, 2002; *Chung et al.*, 2003; *Feely et al.*, 2004]. The change in TA* with chlorofluorocarbon (CFC) age along an isopycnal surface has been interpreted as a measure of the in situ rate of $CaCO_3$ dissolution in the thermocline. The aim of the present study is to evaluate this method of estimating $CaCO_3$ dissolution. Our hypothesis is that a substantial fraction of the TA* burden above the saturation horizon is derived from $CaCO_3$ that was dissolved below the saturation horizon and transported upward. We evaluate this hypothesis by developing and examining a global three-dimensional model of the cycling and distribution of calcium carbonate in the modern open ocean. Our focus is on the Pacific Ocean, which, because of its size, is globally significant. Furthermore, the concentrations of thermocline TA* are high in the Pacific, in contrast to the Atlantic, and

[1]Department of Meteorology, Pennsylvania State University, University Park, Pennsylvania, USA.
[2]Now at DECHEMA Gesellschaft für Chemische Technik und Biotechnologie e.V., Frankfurt, Germany.
[3]Department of Earth, Atmosphere and Planetary Sciences, Massachusetts Institute of Technology, Cambridge, Massachusetts, USA.

0886-6236/06/2006GB002727$12.00

so the error in the method due to measurement error is relatively small. In section 2 we describe the model, which includes an explicit representation of calcium carbonate formation and dissolution, with the latter only occurring below the saturation horizon. In section 3 we demonstrate that the model qualitatively captures the broad-scale observed oceanic distributions of total alkalinity and TA*. We show that the modeled relationship between TA* and CFC age in the thermocline is consistent with that observed, but also that this relationship cannot be interpreted in terms of in situ dissolution above the saturation horizon since this does not occur in this model (section 4). Finally, in section 5, we discuss potential model biases and place our results in a broader context of observations of the marine $CaCO_3$ cycle.

2. Ocean Circulation and Biogeochemistry Model

[5] We use the MIT ocean circulation model [*Marshall et al.*, 1997a, 1997b], which is configured globally at coarse resolution (2.8° × 2.8°, 15 vertical levels) and is forced with a climatological annual cycle of surface wind stresses [*Trenberth et al.*, 1989], heat and freshwater fluxes [*Jiang et al.*, 1999], with additional relaxation toward climatological sea surface temperature and salinity [*Levitus and Boyer*, 1994; *Levitus et al.*, 1994]. The large-scale effects of mesoscale eddy transfers are parameterized following *Gent and McWilliams* [1990] and we impose a globally uniform, background vertical mixing rate for tracers (salt, temperature and biogeochemical) of 0.5×10^{-4} m^2 s^{-1}. Dilution of alkalinity and dissolved inorganic carbon due to net surface freshwater fluxes is represented as a "virtual flux" [*Murnane et al.*, 1999]. We overlay representations of the coupled biogeochemical cycles of carbon, phosphorus, oxygen, and alkalinity (aspects of which are described by *McKinley et al.* [2004] and *Dutkiewicz et al.* [2005]). Biogeochemical tracers are transported by the circulation model's flow field and mixing coefficients using a flux limiter advection scheme [*Roe*, 1985]. We apply a highly idealized parameterization of net community production (B), limited by the availability of photosynthetically active radiation (I), and phosphate,

$$B = \alpha \frac{I}{I + K_I} \frac{PO_4}{PO_4 + K_{PO4}}, \tag{2}$$

where $\alpha = 3$ μM P yr^{-1} is the maximum community production, and the half-saturation coefficients are $K_I = 30$ W m^{-2} and $K_{PO4} = 0.5$ μM. Two thirds of net production is assumed to enter a dissolved organic pool that has an e-folding timescale for remineralization of 6 months [*Yamanaka and Tajika*, 1997]. The remaining fraction of organic production is exported to depth as sinking particles, where it is remineralized according to the empirical power law of *Martin et al.* [1987]. Incident photosynthetically active radiation is determined as a function of latitude and day of year using the astronomical formula of *Paltridge and Platt* [1976] and is attenuated in the water column assuming a uniform extinction coefficient. Transformation of carbon and oxygen to and from organic form are linked to those of phosphorus assuming fixed Redfield stoichiometry. The partitioning of dissolved inorganic carbon is solved explicitly [*Follows et al.*, 2006] and the air-sea exchange of CO_2 is parameterized with a wind-speed dependent gas transfer coefficient following *Wanninkhof* [1992]. The rain ratio, or euphotic zone export of calcium carbonate relative to particulate organic carbon, is imposed using the region-specific estimates of *Sarmiento et al.* [2002].

2.1. Calcium Carbonate Dissolution

[6] We implement a mechanistic formulation of the cycling of calcium carbonate such that dissolution only occurs below the saturation horizon of calcite. We consider only the calcitic form of $CaCO_3$, the dominant form produced in the open ocean [e.g., *Milliman*, 1993; *Fabry*, 1990]. Exported $CaCO_3$ particles are assumed to sink at 100 m d^{-1} and dissolve on the basis of the local saturation state with respect to calcite,

$$\Omega = \frac{[Ca^{2+}][CO_3^{2-}]}{K_{sp}}, \tag{3}$$

where K_{sp} (T, S, p) is the solubility product from *Mucci* [1983] with the pressure dependency of *Millero* [1995]. The concentration of Ca^{2+} is determined assuming a conservative relationship with salinity, $[Ca^{2+}] = 0.01028\ S/35$ mol kg^{-1} [*Department of Energy*, 1994]; since calcium is a major constituent of sea water, it is minimally affected by dissolution of $CaCO_3$. The three-dimensional distribution of $[CO_3^{2-}]$ is computed using the scheme of *Follows et al.* [2006] with pressure dependence of the carbonate system parameters [*Culberson and Pytkowicz*, 1968; *Takahashi et al.*, 1981]. Since the saturation horizon occurs in the deep ocean where temporal variations are small, particularly at the coarse resolution of our model, Ω is evaluated on a monthly basis, significantly reducing total computational cost. The dissolution rate of calcium carbonate below the saturation horizon ($\Omega < 1$) follows the dissolution kinetics determined by *Keir* [1980]:

$$\text{Calcite dissolution rate}\left(\%\ \text{day}^{-1}\right) = 7.177(1 - \Omega)^{4.54}. \tag{4}$$

[7] If calcium carbonate reaches the model ocean floor and $\Omega < 1$, all carbonate particles are immediately dissolved in the local grid cell. If carbonate particles reach the bottom layer and $\Omega > 1$, it is assumed buried. To maintain the global budget of alkalinity, we balance this loss in a highly idealized manner by imposing a source of equal magnitude in the local surface ocean. Note that this source occurs in the surface layer of the model and therefore affects TA^o, but has no impact on TA* (this is important for inferences made later).

2.2. Other Tracers

[8] We also implement two additional, idealized passive tracers to aid the interpretation and illustration of the processes that regulate deep ocean alkalinity in the model. In observational analyses, TA^o is typically estimated using

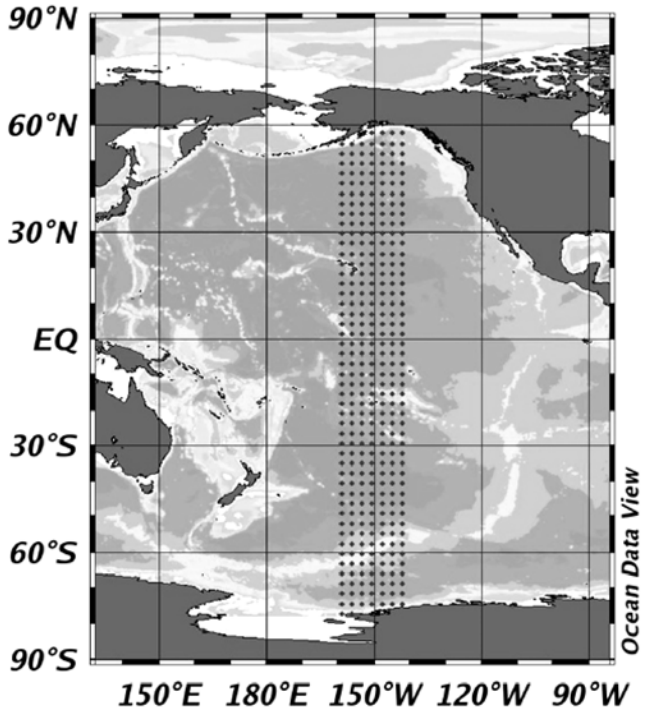

Figure 1. Meridional swath in the modeled Pacific Ocean examined in this manuscript. The grid points are further on treated in the graphs as if being hydrographic stations including samples, i.e., showing the averaged properties of a cell around the cell center.

empirical relationships between surface TA, nutrients, oxygen, temperature and salinity. In the model we have the opportunity to carry an exact tracer of preformed alkalinity, which avoids the uncertainties introduced by the assumed relationships. The exact preformed alkalinity tracer, TA^o, is set equal to the local alkalinity in the surface layer of the model at each time step and has no sources and sinks at depth,

$$TA^o = TA \qquad (0-50\ \text{m}). \tag{5}$$

[9] A second idealized tracer, M, is used to illustrate the effects of transport on a tracer which has an interior ocean source below the saturation horizon and a surface sink,

$$M = 0 \qquad (0-50\ \text{m}) \tag{6}$$

$$M = 100 \qquad \text{if } \Omega < 1. \tag{7}$$

These tracers are also advected and diffused by the circulation model.

[10] Finally, as a measure of the ventilation of thermocline and deep waters in the model and to evaluate the tracer-based method for estimating $CaCO_3$ dissolution, we also perform a simulation of the transient uptake of CFC-12 following the OCMIP-2 protocols [*Dutay et al.*, 2002].

2.3. Spin-Up

[11] The model is initialized with observed distributions of relevant tracers and integrated for several thousand years with atmospheric pCO_2 fixed at the preindustrial mixing ratio 278 ppmv. The biogeochemical tracers, including TA^o and M, are at equilibrium after this long integration. The modeled, steady state distributions of phosphate, oxygen, and preindustrial dissolved inorganic carbon and air-sea CO_2 flux (not shown) qualitatively capture the expected broad-scale features and gradients observed in the modern ocean, similar to previous versions of the MIT model.

3. Model Evaluation

3.1. Observed and Modeled Alkalinity

[12] We now compare the total alkalinity and TA* from the model with observations, focusing on a meridional section through the Pacific (Figure 1). We find that observed [*Key et al.*, 2004] and modeled alkalinities exhibit very similar spatial patterns (Figure 2). In particular, both show: (1) an alternating pattern of alkalinity at the sea surface, reflecting air-sea fresh water fluxes; (2) the signal of low-salinity Antarctic Intermediate Water (AAIW) and North Pacific Intermediate Water; (3) homogenous alkalinity below 1000 m and south of 50°S; (4) an alkalinity maximum associated with old mid-depth waters (~3000 m); and (5) lower-alkalinity Antarctic Bottom Water (AABW) spreading northward along the bottom.

[13] The model shows a number of deficiencies as well. First, the modeled alkalinity is systematically lower than the observations for most of the Pacific by about 50 μmol kg^{-1}. This is in part because the waters below 1500 m are on the average less saline by ~0.3 psu in the model while also being slightly colder. This does not dramatically affect the circulation because of compensating effects on density, but it has a substantial impact on the alkalinity. One unit of salinity change due to freshwater fluxes changes the alkalinity by about 60 μmol kg^{-1}. A second deficiency in the model alkalinity distribution is the absence at mid-depths of the alkalinity maxima around 35°S and the equator evident in the observations. This may be because we represent only one biogenic carbonate mineral (calcite); i.e., aragonite production may be substantial at these latitudes [*Milliman*, 1993] and the saturation horizon for aragonite is shallower than that of calcite [e.g., *Feely et al.*, 2002].

[14] Figure 2 also shows the modeled and observed saturation horizon. Although anthropogenic CO_2 has resulted in shoaling [*Feely et al.*, 2002], it is relatively modest, which allows us to legitimately compare the pre-anthropogenic model with modern observations. The model saturation horizon compares reasonably well with observations, located at around 3000 m south of 30°S and about 1000 m north of 20°N. The model saturation horizon shoals gradually between these two latitudes whereas the observed saturation horizon does so abruptly at around 15°N when assuming that the calculated saturation horizon according to *Mucci* [1983] is without any uncertainty. The shown uncertainty of the saturation horizon that is drawn in Figure 2 is based on recent studies [*Gehlen et al.*, 2005]. This uncer-

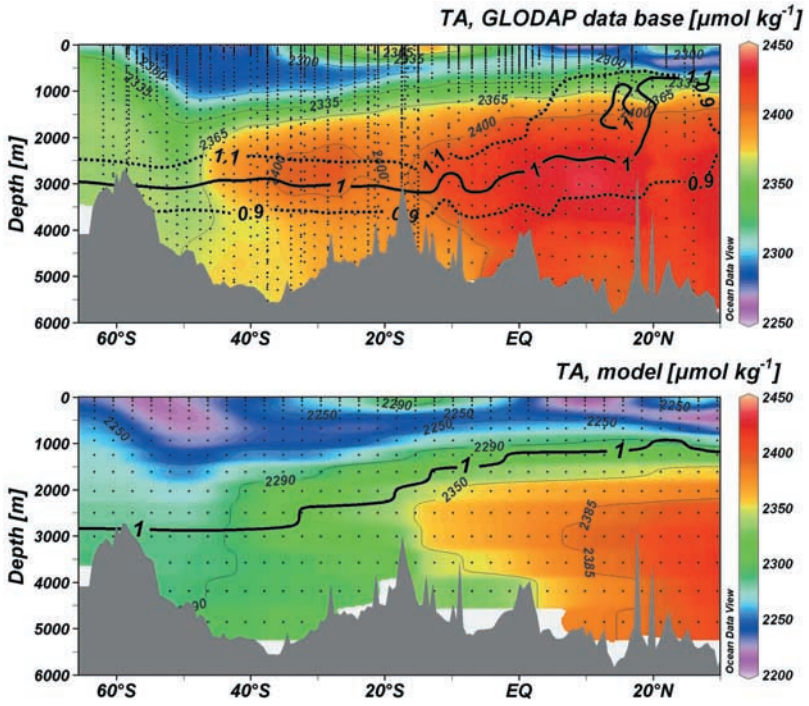

Figure 2. Distribution of alkalinity along the WOCE P16 section to 30°N. Both plots also indicate the saturation horizons for calcite ($\Omega = 1$). Please note the scale change of +50 μmol kg^{-1} from the top plot to the bottom plot. (top) Observations from the GLODAP database [*Key et al.*, 2004]. The uncertainty of the depth of the calcite saturation horizon is about ±10 % for the observations (see section 4.3.) and is also indicated. (bottom) Model.

tainty is discussed in more detail with the potential model biases in section 4.3. At this point we only want to note that it is important to consider the uncertainty in the saturation horizon when interpreting the observed distribution of (excess) alkalinity. The model saturation horizon may be too deep at low latitudes for the same reason that it misses the alkalinity maximum around the equator: the lack of aragonite.

[15] Because TA* quantifies the amount of dissolution of $CaCO_3$ that has occurred in a water parcel since it left the surface, it is perhaps the most relevant tracer for evaluating a model of $CaCO_3$ cycling. To compute TA* in the model, we remove effects of organic matter remineralization, TA^{AOU}, and preformed effects (equation (1)). The former is estimated from the apparent oxygen utilization ($AOU = O_2^{sat}(\theta, S) - O_2$) and the titration stoichiometry of total alkalinity as imposed in the model ($TA^{AOU} = -17/170$ AOU) [*Brewer and Goldman*, 1976]. Equation (1) is thus rearranged to yield

$$TA^* = \frac{1}{2}\left(TA - TA^0 + \frac{17}{170}\,AOU\right), \qquad (8)$$

where all of the tracers on the right hand side are from the model.

[16] The distribution of TA* in the Pacific basin of the model is very similar to that deduced from observations (Figure 3) in both magnitude and distribution pattern. All of the major features are captured, including the middepth maximum north of 40°S, the low values in the thermocline of the southern subtropical gyre, and the low values associated with AAIW and AABW. Negative values in the observational analysis reflect uncertainties in the accuracy of the empirical regression used for preformed alkalinity. The model has somewhat higher values in the deep northern end of the transect, which might be explained by the model's exclusive production of calcite only. If we had included aragonite, we would expect to find smaller differences between model and observations because this $CaCO_3$ would dissolved higher in the water column, leaving less $CaCO_3$ to dissolve at depth and lower TA* there.

[17] In both observations and model there is substantial TA* above the calcite saturation horizon. This result is particularly significant because in the model there is no dissolution above the saturation horizon and thus TA* at shallow depths in the model must reach there by advection and mixing. The diagnostic mixing tracer, *M*, which has a source in the model below the saturation horizon and a sink at the surface, highlights this point (Figure 3, bottom). This clearly illustrates that a tracer like TA*, which is set to zero at the surface and has a source at depth, is ultimately transported into the thermocline.

3.2. Ocean Ventilation and Relationship Between TA* and CFC Age

[18] The CFC age is determined by linking the CFC-12 partial pressure in a water sample to the year where it had this partial pressure in the atmosphere [after *Key et al.*,

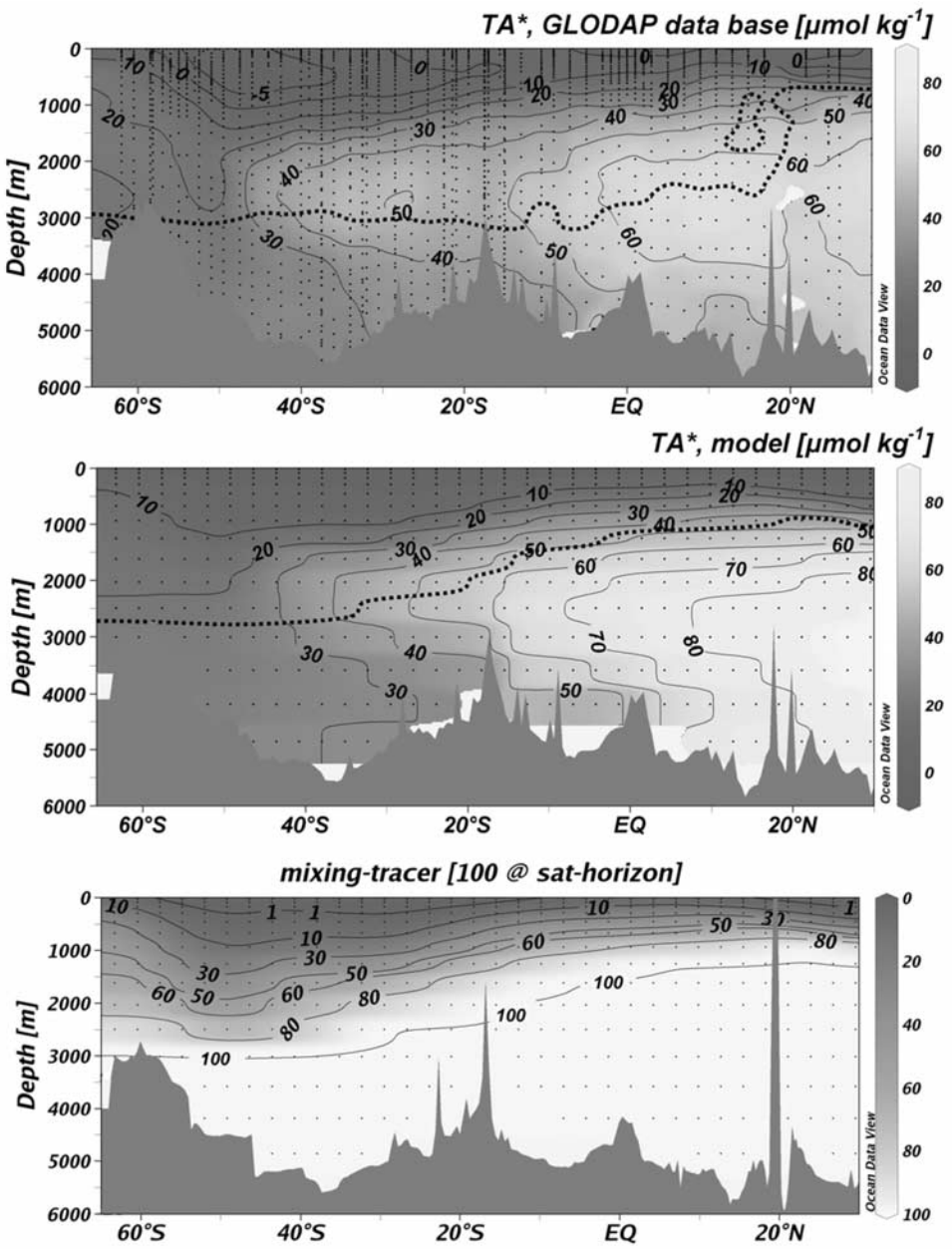

Figure 3. TA* and mixing tracer, *M*, along the WOCE P16 section to 30°N. Dotted lines are the calcite saturation horizons. (top) TA* as derived from observations using the formulas of *Feely et al.* [2002]. (middle) Modeled TA* (equation (8)). (bottom) Mixing tracer, *M*, set to 100 at the calcite saturation horizon and 0 in the surface layer.

2004]. The CFC-12 age provides only an approximate measure of the time since a water parcel was at the surface because each water parcel actually reflects contributions from many pathways through the ocean and thus a spectrum of ages [*Hall and Haine*, 2002]. We use CFC-12 ages only between 0 to 30 years in an effort to minimize errors due to nonlinear mixing. As shown in Figure 4, the model and observations exhibit several similar features in the CFC-12 age distribution: (1) high ages at the equator and subpolar North Pacific and low ages in the subtropical North Pacific, which reflects the Ekman circulation; (2) deeper isolines in the South Pacific than in the North Pacific at similar latitudes, presumably reflecting the hemispheric asymmetry in deep and intermediate water formation; and (3) a very accurate simulation of the 10-year isoline. The model, however, shows lower ages than the observations at most depths below the 10-year isoline (e.g., the 20-year isoline at 50°S is too deep by about 300 m), indicating that the model's upper ocean circulation (advection, mixing or both) at the decadal timescale is somewhat too vigorous.

[19] The relationship between modeled TA* and CFC-12 age above the saturation horizon in the Pacific basin

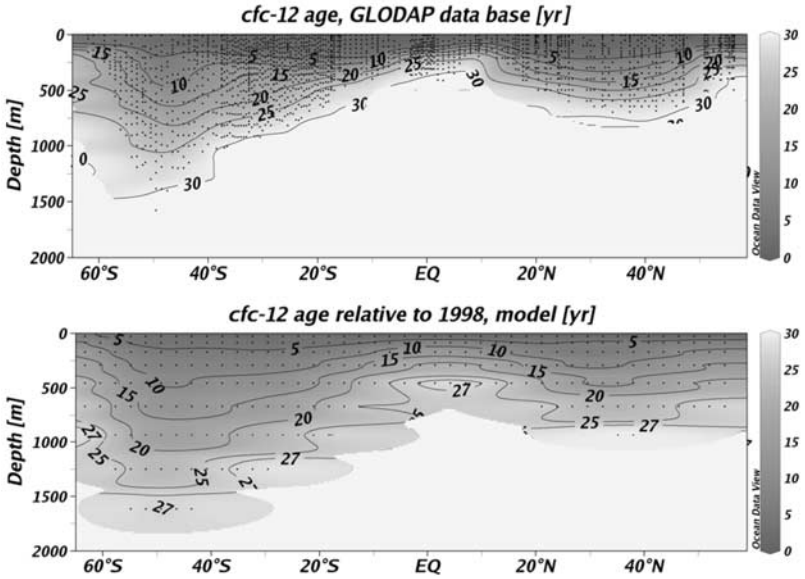

Figure 4. CFC-12 age along the WOCE P16 section. (top) Observed. (bottom) Modeled.

(Figure 5) is qualitatively consistent with that from the observational analysis of *Feely et al.* [2002, Figure 8] with higher values of TA* associated with older, deeper waters. This agreement, combined with the reasonably good simulations of TA, TA* and the saturation horizon, suggest that the model is capturing the key processes controlling the production and dissolution of $CaCO_3$ in the ocean. In particular, the model suggests that traditional, thermodynamically driven $CaCO_3$ dissolution kinetics are consistent with observations of alkalinity.

4. Results and Discussion

4.1. Apparent Dissolution Rates

[20] Previous observational studies [*Feely et al.*, 2002; *Sabine et al.*, 2002; *Chung et al.*, 2003; *Feely et al.*, 2004] estimated $CaCO_3$ dissolution using the relationship between TA* and CFC-12 age. Specifically, TA* was plotted as a function of CFC-12 age, and a line was fit to the data. The slope of this line was interpreted as the average $CaCO_3$ dissolution rate on the isopycnal surface. We have treated the model data in a similar, though not identical fashion. In Figure 5, we plot model TA* versus CFC age along the transect (Figure 1) where we can compute a CFC age (i.e., where the age is less than 30 years), and for points above the saturation horizon. The latter constrains model estimates to the upper 900 m in the North Pacific. For each grid point in the model, we compute the dissolution rate as TA* divided by the CFC-age. We then average those rates as a function of depth in the North and South Pacific and present the results in Figure 6. These rates are compared with revised tracer-based estimates of $CaCO_3$ dissolution from W. M. Berelson et al. (Relating estimates of $CaCO_3$ production, export, and dissolution in the water column to measurements of $CaCO_3$ rain into sediment traps and dissolution on the sea floor: A revised global carbonate budget, submitted to *Global Biogeochemical Cycles*, 2006) (hereinafter referred to as Berelson et al., submitted manuscript, 2006), which were derived from the original measurements of *Feely et al.* [2002]. The mean dissolution rate estimated by Berelson et al. (submitted manuscript, 2006) for the Pacific Ocean between 200 and 1000 m is 0.44 μmol kg^{-1} yr^{-1} (0.79 μmol kg^{-1} yr^{-1} in the North Pacific and 0.22 μmol kg^{-1} yr^{-1} in the South Pacific). The main point is that the rates estimated from the model output are of the same order as those estimated from observations. However, since there is no calcium carbonate dissolution above the saturation horizon in the model, the estimated rate in the model cannot be attributed to local dissolution. Since there are no local sources and sinks of TA* or CFC-12 in the thermocline of the model, the relationship must be explained by ocean transport leading to a comingling of the two tracers.

4.2. Ocean Transport of TA*

[21] The saturation horizon does not follow isopycnal surfaces and gradients in TA* can form along deep ocean isopycnals that cross the saturation horizon (Figure 7). TA* can thus be transported isopycnally, by advection or eddy stirring, to above the saturation horizon (Figure 8). The isopycnals of the main thermocline may never intercept the saturation horizon but TA* can also be transported onto these density surfaces by the relatively slow, but ubiquitous, diapycnal mixing [e.g., *Munk and Wunsch*, 1998]. Likewise, these isopycnal and diapycnal transport processes ventilate CFC-12 into the thermocline and deep ocean from the surface. We can thus explain why the apparent dissolution rates are on the average higher in the North Pacific than in the South Pacific: The carbonate saturation horizon shoals to the north so advection and/or mixing along isopycnals easily leads to a mingling of TA*, from below, and CFC-12, from above.

[22] In the numerical model these transport processes must be sufficient to account for the TA* signature above

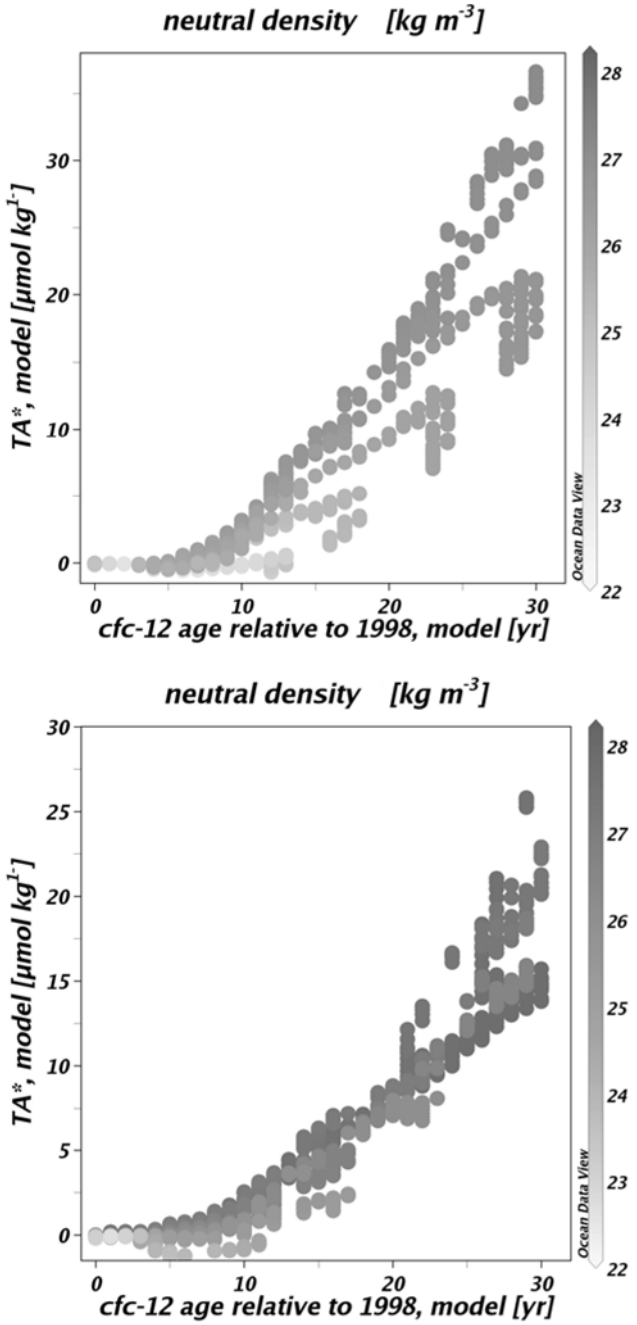

Figure 5. Modeled TA* versus CFC-12 age. Shading indicates neutral density. (top) North Pacific. (bottom) South Pacific. Only values from the gridpoints in Figure 1 that are above the saturation horizon are shown.

the saturation horizon. A simple scale analysis demonstrates that this is plausible both for the modeled and observed ocean. The prognostic equation for alkalinity in the ocean is

$$\frac{\partial \mathrm{TA}}{\partial t} = -\mathbf{u}\cdot\nabla \mathrm{TA} + \nabla\cdot(K\nabla \mathrm{TA}) + J^{*} + J^{\mathrm{AOU}}, \qquad (9)$$

where the first two terms are advection and diffusion, respectively; J^{*} is the formation and dissolution of calcium carbonate; and J^{AOU} is the contribution due to the production and remineralization of organic matter. TA is a linear combination of TA^{o}, TA*, and $\mathrm{TA}^{\mathrm{AOU}}$ (from equation (1)) so we may treat TA* separately,

$$\frac{\partial \mathrm{TA}^{*}}{\partial t} = -\mathbf{u}\cdot\nabla \mathrm{TA}^{*} + \nabla\cdot(K\nabla \mathrm{TA}^{*}) + J^{*}. \qquad (10)$$

[23] Consider the steady state in the ocean interior, away from the surface sinks and deep sources of TA*, such as within the main thermocline. The magnitude of the contributions from each transport term may be evaluated from the observed or modeled gradients of TA*, current speeds and mixing rates. Let us consider also an isopycnic framework where, from the observations and model, we estimate that a change in TA*, $\Delta \mathrm{TA}^{*} \sim 30\ \mu\mathrm{mol\ kg}^{-1}$, occurs over some isopycnic length-scale, $L_i \sim 5000$ km, or diapycnic length scale, $L_d \sim 500$ m. We also assume a reasonable isopycnic current speed, $U_i \sim \mathrm{O}(0.01\ \mathrm{m\ s}^{-1})$, isopycnic mixing rate coefficient, $K_i \sim \mathrm{O}(1000\ \mathrm{m}^2\ \mathrm{s}^{-1})$, and diapycnic mixing rate coefficient, $K_d \sim 0.5 \times 10^{-4}\ \mathrm{m}^2\ \mathrm{s}^{-1}$. The latter is as imposed in the illustrated numerical model configuration; in the ocean this is variable and ranges from ~0.1 to

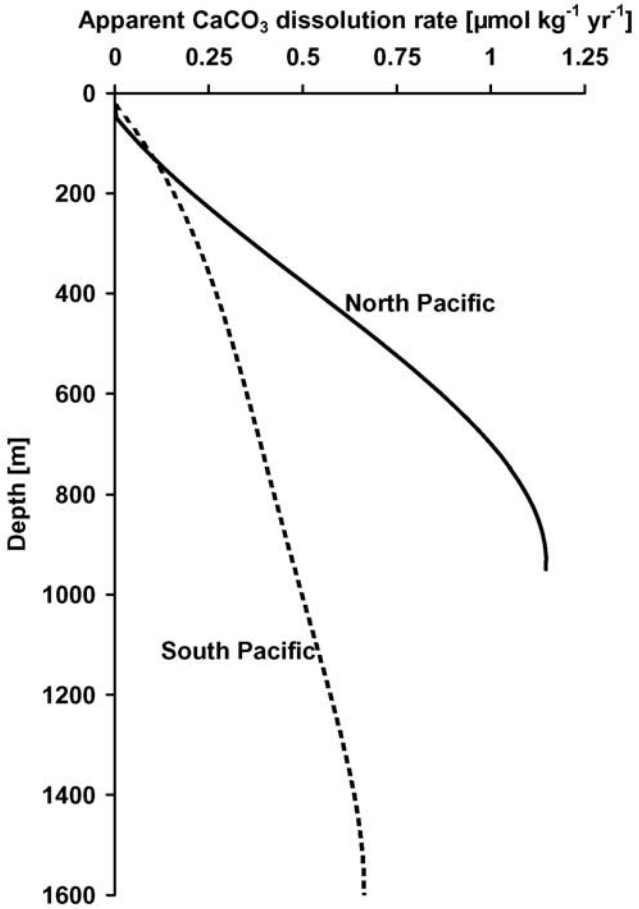

Figure 6. Average profiles of the apparent calcium carbonate dissolution rates, derived from TA* and CFC-12 age in the model at the gridpoints shown in Figure 1. North Pacific, solid lines; South Pacific, dotted lines.

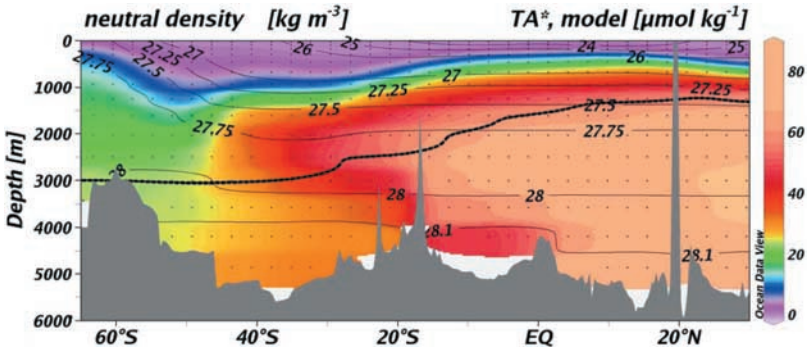

Figure 7. Modeled TA* (shading) and neutral density (isolines) along the WOCE P16 section to 30°N. The thick dotted line is the calcite saturation horizon.

$\sim 100 \times 10^{-4}$ m^2 s^{-1} [*Garabato et al.*, 2004]. Evaluating the transport contributions yields

$$0 = -\frac{U_i}{L_i}\Delta \mathrm{TA}^* + \frac{K_i}{L_i^2}\Delta \mathrm{TA}^* + \frac{K_d}{L_d^2}\Delta \mathrm{TA}^* + J^*. \qquad (11)$$

Estimating typical values for the transport terms on the right-hand side of equation (11) we find ~ 0.6 μmol kg^{-1} yr^{-1} for isopycnal advection (first term), ~ 0.01 μmol kg^{-1} yr^{-1} for isopycnal mixing (second term), and ~ 0.1 μmol kg^{-1} yr^{-1} for diapycnal mixing (third term). Thus, on the basis of the magnitude of observed gradients, current speeds and mixing rates, ocean transport contributions are of the same order of magnitude as the apparent ''source'' of TA* in the thermocline using the relationship between TA* and CFC age. This highly simplified scale analysis suggests that isopycnal advection and diapycnal mixing are likely the most significant contributions (certainly in the numerical model). In the ocean, the inhomogeneity of both isopycnal and diapycnal mixing rates, as well as TA* gradients, will lead to significant variation in the relative contributions.

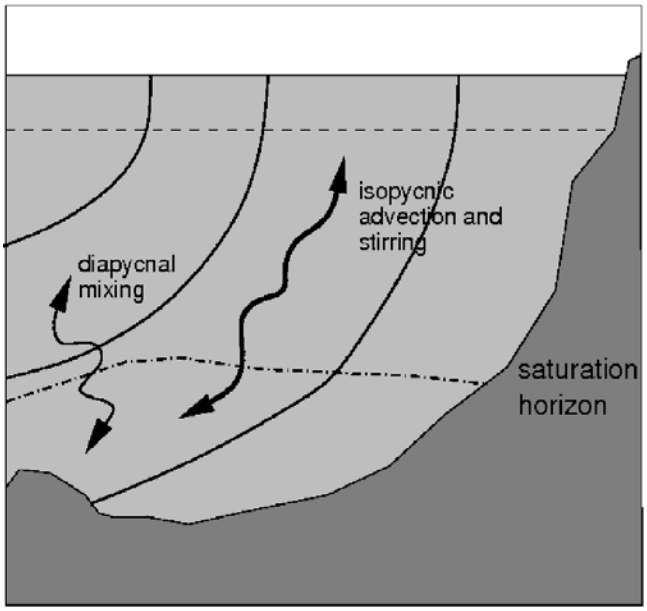

Figure 8. Schematic depiction of the pathways by which TA* is transported to depths above the saturation horizon. This can occur by isopycnic stirring or advection along a density surface, which intercepts the saturation horizon, or by diapycnal mixing.

4.3. Potential Biases of the Model and Saturation Horizon Uncertainty

[24] There are a number of reasons why we may have overestimated the transport artifact in the tracer-based method of *Feely et al.* [2002], *Sabine et al.* [2002], *Chung et al.* [2003] and *Feely et al.* [2004]. First, the value of the diapycnal mixing coefficient used in the model (0.5×10^{-4} m^2 s^{-1}) is substantially greater than what direct measurements based on purposeful tracer experiments in the pycnocline away from boundaries suggest, $\sim 0.1-0.2 \times 10^{-4}$ m^2 s^{-1} [*Watson and Ledwell*, 2000, and references therein]. We ran the biogeochemical model offline with the same circulation field but with diapycnal diffusivity reduced to 0.25×10^{-4} m^2 s^{-1}. The resulting fields of TA* and M (auxiliary material[1] Figure S1) are very similar to those produced with the standard, higher mixing case. We thus conclude that the higher-than-observed diapycnal mixing in the model is not a serious limitation of our study. Nevertheless, the CFC tracer provides compelling evidence that the upper ocean circulation in the model is too vigorous, which may produce a significant bias in our result. This will require further study with models that have a more realistic ventilation of the thermocline.

[25] Another potential bias in the model is due to its lack of aragonite. We argued above that deficiencies in the modeled alkalinity distribution may be due to this omission. Including aragonite might also reduce the transport artifact in the tracer-based method. This is because aragonite dissolving above the calcite saturation horizon would reduce TA* gradients across the saturation horizon, and thus reduce the transport of TA* to undersaturated waters. However, because aragonite production is only roughly 10% of carbonate production globally, we doubt this is a significant limitation.

[1]Auxiliary materials are available in the HTML. doi:10.1029/2006GB002727.

[26] A more significant limitation may be that our saturation horizon is too shallow in the tropical ocean, which means that TA* is produced too high in the water column and there may thus be too much transported upward into the thermocline. However, for the observations there is also significant uncertainty in the location of the saturation horizon in the ocean interior. The solubility product of calcite used for observational studies and ours assumes an accuracy of ±5% [*Mucci*, 1983]. However, the measurements by Mucci were all performed at atmospheric pressure and there are additional uncertainties when adjusting the calcite saturation state to greater depth/pressure [*Millero*, 1995], including uncertainty originating from the dissociation constants of carbonic acid. Hence the depth of the saturation horizon is somewhat uncertain and we have indicated a range of ±10% in Figure 2. This is in agreement with a recent study by *Gehlen et al.* [2005], who find calcite solubilities 4%–24% higher than those given by *Mucci* [1983]. Assuming that analytical techniques have advanced in the last 20 years, the true calcite saturation horizon in Figure 2 may be closer to the $\Omega = 1.1$ isoline than the $\Omega = 1.0$ isoline. This also needs to be kept in mind for observations that indicate divergence of the saturation horizon from excess alkalinity patterns as shown in the top plot of Figure 3. In particular, isolated maxima of TA* above the saturation horizon are hard to explain when the uncertainty in the Ω–isoline is not considered. Nonetheless, and as discussed above, such a discrepancy may also be due to our exclusion of aragonite.

4.4. Implications for Shallow Dissolution

[27] *Milliman et al.* [1999] presented a diverse set of observations to make the case for $CaCO_3$ dissolution above the saturation horizon. Qualitative in situ evidence of shallow dissolution, such as etching of $CaCO_3$ surfaces [*Troy et al.*, 1997; *Andruleit*, 2000] and the disappearance of calcite-forming species with depth in the water column, is difficult to dismiss. Decreases with depth in the ratio of $CaCO_3$ flux to the flux of relatively conservative aluminosilicates, as measured by sediment traps [*Martin et al.*, 1993], also supports shallow dissolution, but it is plausible that hydrodynamic and biogenic artifacts that affect trapping efficiency [*Yu et al.*, 2001] could produce such a trend. *Feely et al.* [2004] also summarize evidence of large decreases of $CaCO_3$ flux with depth in sediment traps but advise caution in its interpretation. In support of shallow dissolution, *Milliman et al.* [1999] also summarize measurements of salinity-normalized "excess calcium," which reveal increases with depth across the saturation horizon. This, however, can be explained by the transport arguments we make here, biases associated with the chosen normalization [*Friis et al.*, 2003], and the neglect of removing preformed effects.

[28] Even if we accept the accumulated evidence of *Milliman et al.* [1999], it is nonetheless qualitative. There are two exceptions. First, *Milliman et al.* [1999] compiled sediment trap and calcification rate measurements in the Arabian Sea and find that as much as 70–90% of the production disappears by 800–1000 m. This could perhaps be explained away by an undertrapping problem [*Yu et al.*, 2001], or the dissolution could be occurring exclusively in the euphotic zone, and so would not contribute to the TA* burden of the thermocline. Another quantitative line of evidence is based on the difference between globally averaged 1000-m sediment trap fluxes, estimated by *Milliman* [1993] to be 0.3 Pg C yr^{-1}, and export from the euphotic zone, which *Milliman et al.* [1999] estimate to range from 0.6 to 0.9 Pg C yr^{-1}, suggesting shallow dissolution between 0.3 and 0.6 Pg C yr^{-1}, or 50–70% of surface export. We reassessed the literature on $CaCO_3$ export from the euphotic zone and found an even larger range of estimates: global box and 1-D models give between 0.6 and 1.5 Pg C yr^{-1} [*Garcon and Minster*, 1988; *Shaffer*, 1993; *Chuck et al.*, 2005]; global 3-D models give between 0.4 and 1.8 Pg C yr^{-1} [*Bacastow and Maier-Reimer*, 1990; *Yamanaka and Tajika*, 1996; *Archer et al.*, 1998; *Murnane et al.*, 1999; *Moore et al.*, 2002, 2004]; seasonal alkalinity drawdowns yield 1.4 ± 0.3 Pg C yr^{-1} [*Lee*, 2001]; and PIC:POC export ratios (derived from tracer data) combined with a satellite-derived organic carbon export estimate gives 0.6 Pg C yr^{-1} [*Sarmiento et al.*, 2002]. The overall range is thus 0.4 to 1.8 Pg C yr^{-1}, which, when combined with a recent estimate of 0.4 Pg C yr^{-1} for 2000-m sediment trap fluxes [*Feely et al.*, 2004], yields estimates of dissolution from 0 to 1.4 Pg C yr^{-1}, or 0% to 80% of surface export, a range that is so large as to make compelling statements about shallow dissolution difficult. We feel confident, however, that $CaCO_3$ dissolution on the order of 0.5 μmol kg^{-1} (Figure 6 [see also *Feely et al.*, 2004, Figure 4]) is unrealistically large; this rate, when globally integrated over the upper 1000 m yields around 2 Pg C yr^{-1}.

5. Conclusions

[29] Our study suggests that it is incorrect to interpret the presence of excess dissolved calcium carbonate above the saturation horizon, and its relationship with other tracers such as CFC-age, as an indicator or measure of shallow depth or in situ dissolution of $CaCO_3$. The model presented here reproduces the broad features of observed alkalinity and TA* with no dissolution above the saturation horizon. The presence of TA* in the thermocline and at middepths in the model is demonstrated, through scaling arguments and an idealized tracer study, to be attributable to isopycnal and diapycnal transport in the ocean. These scaling arguments are equally relevant to the observations.

[30] We suggest that recent estimates of significant rates of shallow depth calcium carbonate dissolution in the thermocline are very likely too high because the contribution of transport processes was not adequately accounted for. While we demonstrate that dissolution of calcium carbonate above the saturation horizon need not be invoked in order to understand the observed distribution of TA*, and that transport is particularly significant in the upper ocean, model limitations prevent us from ruling out significant shallow dissolution. We suggest that a rigorous, three-dimensional data assimilation model may be the appropriate framework to resolve this outstanding question.

[31] **Acknowledgments.** We thank the group of lead authors of the Science and three GBC papers, which address excess alkalinity patterns as derived from observations. We are grateful for the data they provided and for their critical reviewer comments on both former manuscripts and conference presentations over the last two and a half years. For this publication, two anonymous reviewers helped to make substantial improvements in the manuscripts. We thank the reviewers for that. K. F. and R. G. N. were supported by NOAA grant GC02-367b and NSF grant OCE-0136621. M. J. F. and S. D. are grateful for support from NOAA and NSF OCE.

References

Anderson, L. A., and J. L. Sarmiento (1994), Redfield ratios of remineralization determined by nutrient data analysis, *Global Biogeochem. Cycles*, *8*, 65–80.

Andruleit, H. A. (2000), Dissolution-affected coccolithophore fluxes in the central Greenland Sea (1994/1995), *Deep Sea Res., Part II*, *47*, 1719–1742.

Archer, D. E., H. Kheshgi, and E. Maier-Reimer (1998), The dynamics of fossil fuel CO_2 neutralization by marine $CaCO_3$, *Global Biogeochem. Cycles*, *12*, 259–276.

Bacastow, R., and E. Maier-Reimer (1990), Ocean-circulation model of the carbon cycle, *Clim. Dyn.*, *4*, 95–125.

Brewer, P. G. (1978), Direct observation of the oceanic CO_2 increase, *Geophys. Res. Lett.*, *5*, 997–1000.

Brewer, P. G., and J. C. Goldman (1976), Alkalinity changes generated by phytoplankton growth, *Limnol. Oceanogr.*, *21*, 108–117.

Broecker, W. S., and T.-H. Peng (1982), *Tracers in the Sea*, Lamont-Doherty Earth Obs., Palisades, N. Y.

Chuck, A., T. Tyrrell, I. J. Totterdell, and P. M. Holligan (2005), The oceanic response to carbon emissions over the next century: investigation using three ocean carbon cycle models, *Tellus, Ser. B*, *57*, 70–86.

Chung, S. N., K. Lee, R. A. Feely, C. L. Sabine, F. J. Millero, R. Wanninkhof, J. L. Bullister, R. M. Key, and T.-H. Peng (2003), Calcium carbonate budget in the Atlantic Ocean based on water column inorganic carbon chemistry, *Global Biogeochem. Cycles*, *17*(4), 1093, doi:10.1029/2002GB002001.

Culberson, C. H., and R. M. Pytkowicz (1968), Effect of pressure on carbonic acid and *p*H in seawater, *Limnol. Oceanogr.*, *13*, 403–411.

Department of Energy (1994), *Handbook of Methods for the Analysis of Various Parameters of the Carbon Dioxide System in Sea Water*, vers. 2.0, edited by A. G. Dickson and C. Goyet, Washington, D. C.

Dutay, J.-C., et al. (2002), Evaluation of ocean model ventilation with CFC-11: Comparison of 13 global ocean models, *Ocean Modell.*, *4*, 89–120.

Dutkiewicz, S., M. J. Follows, and P. Parekh (2005), Interactions of the iron and phosphorus cycles: A three-dimensional model study, *Global Biogeochem. Cycles*, *19*, GB1021, doi:10.1029/2004GB002342.

Fabry, V. J. (1990), Shell growth-rates of pteropod and heteropod mollusks and aragonite production in the open ocean—Implications for the marine carbonate system, *J. Mar. Syst.*, *48*(1), 209–222.

Feely, R. A., et al. (2002), In situ calcium carbonate dissolution in the Pacific Ocean, *Global Biogeochem. Cycles*, *16*(4), 1144, doi:10.1029/2002GB001866.

Feely, R. A., C. L. Sabine, K. Lee, W. Berelson, J. Kleypas, V. J. Fabry, and F. J. Millero (2004), Impact of anthropogenic CO_2 on the $CaCO_3$ system in the oceans, *Science*, *305*, 362–366.

Follows, M. J., S. Dutkiewicz, and T. Ito (2006), On the solution of the carbonate system in ocean biogeochemistry models, *Ocean Modell.*, *12*, 290–301.

Friis, K., A. Körtzinger, and D. W. R. Wallace (2003), The salinity normalization of marine inorganic carbon chemistry data, *Geophys. Res. Lett.*, *30*(2), 1085, doi:10.1029/2002GL015898.

Garabato, A. C. N., K. L. Polzin, B. A. King, K. J. Heywood, and M. Visbeck (2004), Widespread intense turbulent mixing in the Southern Ocean, *Science*, *303*, 210–213.

Garcon, V. C., and J.-F. Minster (1988), Heat, carbon and water fluxes in a 12-box model of the world ocean, *Tellus, Ser. B*, *40*, 161–177.

Gehlen, M., F. C. Bassinot, L. Chou, and D. McCorkle (2005), Reassessing the dissolution of marine carbonates: I. Solubility, *Deep Sea Res., Part I*, *52*, 1445–1460.

Gent, P., and J. McWilliams (1990), Isopycnal mixing in ocean circulation models, *J. Phys. Oceanogr.*, *20*, 150–155.

Hall, T. M., and T. W. N. Haine (2002), On ocean transport diagnostics: The idealized age tracer and the age spectrum, *J. Phys. Oceanogr.*, *32*, 1987–1991, doi:10.1175/1520-0485.

Jiang, S., P. H. Stone, and P. Malanotte-Rizzoli (1999), An assessment of the Geophysical Fluid Dynamics Laboratory ocean model with coarse resolution: Annual-mean climatology, *J. Geophys. Res.*, *104*, 25,623–25,645.

Keir, R. S. (1980), The dissolution kinetics of biogenic calcium carbonates in seawater, *Geochim. Cosmochim. Acta*, *44*, 241–252.

Key, R. M., A. Kozyr, C. L. Sabine, K. Lee, R. Wanninkhof, J. L. Bullister, R. A. Feely, F. J. Millero, C. Mordy, and T.-H. Peng (2004), A global ocean carbon climatology: Results from Global Data Analysis Project (GLODAP), *Global Biogeochem. Cycles*, *18*, GB4031, doi:10.1029/2004GB002247.

Lee, K. (2001), Global net community production estimated from the annual cycle of surface water total dissolved inorganic carbon, *Limnol. Oceanogr.*, *46*, 1287–1297.

Levitus, S., and T. P. Boyer (1994), *World Ocean Atlas 1994*, vol. 4, *Temperature, NOAA Atlas NESDIS 4*, 117 pp., Natl. Oceanic and Atmos. Admin., Silver Spring, Md.

Levitus, S., R. Burgett, and T. P. Boyer (1994), *World Ocean Atlas 1994*, vol. 3, *Salinity, NOAA Atlas NESDIS 3*, 99 pp., Natl. Oceanic and Atmos. Admin., Silver Spring, Md.

Lohmann, G. P. (1995), A model for variation in the chemistry of planktonic foraminifera due to secondary calcification and selective dissolution, *Paleoceanography*, *10*, 445–457.

Marshall, J., A. Adcroft, C. Holl, L. Perelman, and C. Heisey (1997a), A finite-volume, incompressible Navier Stokes model for studies of the ocean on parallel computers, *J. Geophys. Res.*, *102*, 5753–5766.

Marshall, J., C. Hill, L. Perelman, and A. Adcroft (1997b), Hydrostatic, quasi-hydrostatic, and nonhydrostatic ocean modeling, *J. Geophys. Res.*, *102*, 5733–5752.

Martin, J., G. Knauer, D. Karl, and W. Broenkow (1987), VERTEX: Carbon cycling in the northeast Pacific, *Deep Sea Res.*, *Part I*, *34*, 267–285.

Martin, J., S. E. Fitzwater, R. M. Gordon, C. N. Hunter, and S. J. Tanner (1993), Iron, primary production and carbon-nitrogen flux studies during the JGOFS North Atlantic Bloom Experiment, *Deep Sea Res.*, *Part II*, *40*, 115–134.

McKinley, G. A., M. J. Follows, and J. Marshall (2004), Mechanisms of air-sea CO_2 flux variability in the equatorial Pacific and the North Atlantic, *Global Biogeochem. Cycles*, 18, GB2011, doi:10.1029/2003GB002179.

Millero, F. J. (1995), The thermodynamics of the carbonate system in the oceans, *Geochim. Cosmochim. Acta*, *59*, 661–677.

Milliman, J. D. (1993), Production and accumulation of calcium carbonate in the ocean: Budget of a nonsteady state, *Global Biogeochem. Cycles*, *7*, 927–957.

Milliman, J. D., and A. W. Droxler (1996), Neritic and pelagic carbonate sedimentation in the marine environment: Ignorance is not bliss, *Geol. Rundsch.*, *85*(3), 496–504.

Milliman, J. D., P. J. Troy, W. M. Balch, A. K. Adams, Y. H. Li, and F. T. Mackenzie (1999), Biologically mediated dissolution of calcium carbonate above the chemical lysocline?, *Deep Sea Res., Part I*, *46*, 1653–1669.

Moore, J. K., S. C. Doney, D. M. Glover, and I. Y. Fung (2002), Iron cycling and nutrient limitation patterns in surface waters of the world ocean, *Deep Sea Res., Part II*, *49*, 463–508.

Moore, J. K., S. C. Doney, and K. Lindsay (2004), Upper ocean ecosystem dynamics and iron cycling in a global three-dimensional model, *Global Biogeochem. Cycles*, 18, GB4028, doi:10.1029/2004GB002220.

Mucci, A. (1983), The solubility of calcite and aragonite in seawater at various salinities, temperatures and one atmosphere total pressure, *Am. J. Sci.*, *283*, 780–799.

Munk, W. H., and C. Wunsch (1998), Abyssal recipes II: Energetics of tidal and wind mixing, *Deep Sea Res., Part I*, *45*, 1977–2010.

Murnane, R. J., J. L. Sarmiento, and C. Le Quéré (1999), Spatial distribution of air-sea CO_2 fluxes and the interhemispheric transport of carbon by the oceans, *Global Biogeochem. Cycles*, *13*, 287–305.

Paltridge, G., and C. Platt (1976), *Radiative Processes in Meteorology and Climatology*, Elsevier, New York.

Roe, P. (1985), Some contributions to the modeling of discontinuous flows, in *Large-Scale Computations in Fluid Mechanics*, edited by B. Engquist, S. Osher, and R. Somerville, pp. 163–193, Am. Math. Soc., Providence, R. I.

Sabine, C. L., R. M. Key, R. A. Feely, and D. Greeley (2002), Inorganic carbon in the Indian Ocean: Distribution and dissolution processes, *Global Biogeochem. Cycles*, *16*(4), 1067, doi:10.1029/2001GB001869.

Sarmiento, J. L., J. Dunne, A. Gnanadesikan, R. M. Key, K. Matsumoto, and R. Slater (2002), A new estimate of the $CaCO_3$ to organic carbon export ratio, *Global Biogeochem. Cycles*, *16*(4), 1107, doi:10.1029/2002GB001919.

Schiebel, R. (2002), Planktonic foraminiferal sedimentation and the marine calcite budget, *Global Biogeochem. Cycles*, *16*(4), 1065, doi:10.1029/2001GB001459.

Shaffer, G. (1993), Effects of the marine biota on global carbon cycling, in *The Global Carbon Cycle, NATO ASI Ser.,* vol. I15, *Global Environmental Change*, edited by M. Heimann, pp. 431–455, Springer, New York.

Takahashi, T., W. S. Broecker, and A. E. Bainbridge (1981), The alkalinity and total carbon dioxide concentrations in the world oceans, in *Carbon Cycle Modelling*, edited by B. Bolin, pp. 159–200, John Wiley, Hoboken, N. J.

Trenberth, K., J. Olson, and W. Large (1989), A global ocean wind stress climatology based on ECMWF analyses, *Tech. Rep. NCAR/TN-338+STR*, Natl. Cent. for Atmos. Res., Boulder, Colo.

Troy, P. J., Y.-H. Li, and F. T. Mackenzie (1997), Changes in surface morphology of calcite exposed to the oceanic water column, *Aquat. Geochem.*, *3*, 1–20.

Wanninkhof, R. (1992), Relationship between wind speed and gas exchange over the ocean, *J. Geophys. Res.*, *97*, 7373–7382.

Watson, A. J., and J. R. Ledwell (2000), Oceanographic tracer release experiments using sulfur hexafluoride, *J. Geophys. Res.*, *105*, 14,325–14,337.

Yamanaka, Y., and E. Tajika (1996), The role of the vertical fluxes of particulate organic matter and calcite in the ocean carbon cycle: Studies using an ocean biogeochemical model, *Global Biogeochem. Cycles*, *10*, 361–382.

Yamanaka, Y., and E. Tajika (1997), Role of dissolved organic matter in the marine biogeochemical cycle: Studies using and ocean biogeochemical general circulation model, *Global Biogeochem. Cycles*, *11*, 599–612.

Yu, E.-F., R. Francois, M. P. Bacon, S. Honjo, A. P. Fleer, S. J. Manganini, L. M. M. van der Rutgers, and V. Ittekkot (2001), Trapping efficiency of bottom-tethered sediment traps estimated from the intercepted fluxes of ^{230}Th and ^{231}Pa, *Deep Sea Res., Part I*, *48*, 865–889.

S. Dutkiewicz and M. J. Follows, Massachusetts Institute of Technology, Department of Earth, Atmosphere and Planetary Sciences, 77 Massachusetts Av., Cambridge, MA 02139, USA.

K. Friis, DECHEMA Gesellschaft für Chemische Technik und Biotechnologie e.V., Theodor-Heuss-Allee 25, D-60486 Frankfurt, Germany. (friis@dechema.de)

R. G. Najjar, Department of Meteorology, Pennsylvania State University, 503 Walker Building, University Park, PA 16802-5013, USA.